Competitive balance of intrabulge BMP/Wnt signaling reveals a robust gene network ruling stem cell homeostasis and cyclic activation

Eve Kandyba[a], Yvonne Leung[a], Yi-Bu Chen[b], Randall Widelitz[c], Cheng-Ming Chuong[c], and Krzysztof Kobielak[a,c,1]

[a]Eli and Edythe Broad CIRM Center for Regenerative Medicine and Stem Cell Research, University of Southern California, Los Angeles, CA 90033; [b]Norris Medical Library, University of Southern California, Los Angeles, CA 90033; and [c]Department of Pathology, University of Southern California, Los Angeles, CA 90033

Edited by Mina J. Bissell, E. O. Lawrence Berkeley National Laboratory, Berkeley, CA, and approved November 19, 2012 (received for review January 3, 2012)

Hair follicles facilitate the study of stem cell behavior because stem cells in progressive activation stages, ordered within the follicle architecture, are capable of cyclic regeneration. To study the gene network governing the homeostasis of hair bulge stem cells, we developed a Keratin 15-driven genetic model to directly perturb molecular signaling in the stem cells. We visualize the behavior of these modified stem cells, evaluating their hair-regenerating ability and profile their molecular expression. Bone morphogenetic protein (BMP)-inactivated stem cells exhibit molecular profiles resembling those of hair germs, yet still possess multipotentiality in vivo. These cells also exhibit up-regulation of Wnt7a, Wnt7b, and Wnt16 ligands and Frizzled (Fzd) 10 receptor. We demonstrate direct transcriptional modulation of the *Wnt7a* promoter. These results highlight a previously unknown intra-stem cell antagonistic competition, between BMP and Wnt signaling, to balance stem cell activity. Reduced BMP signaling and increased Wnt signaling tilts each stem cell toward a hair germ fate and, vice versa, based on a continuous scale dependent on the ratio of BMP/Wnt activity. This work reveals one more hierarchical layer regulating stem cell homeostasis beneath the stem cell–dermal papilla-based epithelial–mesenchymal interaction layer and the hair follicle–intradermal adipocyte-based tissue interaction layer. Although hierarchical layers are all based on BMP/Wnt signaling, the multilayered control ensures that all information is taken into consideration and allows hair stem cells to sum up the total activators/inhibitors involved in making the decision of activation.

hair follicle stem cells | β-catenin | BMPR1A

Understanding the basic processes that maintain the homeostasis of adult stem cells (SCs) and how they respond to physiological changes (1) and injury (2) throughout life is of fundamental importance. Regeneration of hair follicles (HFs) is an excellent model because of the distinct topological layout of stem cell populations, their ability to activate cyclically, and their responsiveness to multilayered environmental modulators (3). In adult skin, each HF contains a reservoir of hair follicle stem cells (hfSCs), with label-retaining, slow-cycling cells localized in the bulge (4, 5). hfSCs maintain self-renewal and multipotency in vitro as well as in vivo and are able to regenerate epidermis, HFs, and sebaceous glands (6–8). HFs undergo episodic cycles of growth (anagen), degeneration (catagen), and rest (telogen) (9). Although hfSCs are the main engine that fuels the growth phase, other cells localized in the hair germ (HG) are primed to initiate HF regeneration in response to dermal papilla (DP) signals (10). During the hair cycle, the behavior of slow-cycling hfSCs is tightly governed by an intricate balance of two known signaling pathways [bone morphogenetic protein (BMP) and wingless-type MMTV integration site family (Wnt)] that converge to induce bouts of hfSC quiescence and activation, resulting in new hair formation (11–13).

Apart from the intrafollicular role played by the DP on SCs, extrafollicular s.c. adipose tissue affects hfSC activity via BMPs (13), DKK, Sfrp4 (14), and PDGF (15). Furthermore, hfSCs respond to body hormone status (3) and changes in circadian rhythms (16, 17). Thus, hfSCs present a unique adult stem cell population for us to identify the essential property of a robust gene network capable of maintaining stem cell homeostasis while allowing plasticity to shift between a continuum of quiescent and activated states before becoming irreversibly committed. To be responsive to various physiological conditions, this stem cell gene network module must sense multiple signal inputs. BMP signaling is essential for hair cycling (12, 18–22), and Wnt pathway activation is required to stimulate hair growth (23). Although there is evidence for cross talk between the BMP- and Wnt-signaling pathways in hair follicles (12, 18), direct perturbation of molecular networks within hfSCs in vivo has not been explored.

In this report, we address the underlying molecular mechanisms of BMP signaling in hfSC regulation in vivo. We developed strategies to isolate, characterize, and culture hfSCs where BMP signaling was inactivated. Gene expression data revealed putative in vivo targets of BMP signaling in hfSCs. hfSCs switched from quiescence to activation and acquired molecular characteristics resembling the HG. Interestingly, these activated hfSCs behaved differently from the HG and still maintained characteristics of SCs when cultured in vitro and multipotency after transplantation in vivo. hfSCs with suppressed BMP signaling have altered BMP and Wnt pathway expression. Together, our results suggest an intrinsic mechanism of ligand–receptor-dependent cross talk between BMP and Wnt signaling in hfSC homeostasis.

Results

Use of a Genetic Model to Visualize hfSC Molecular Dynamics with Direct Modulation of BMP Levels in Vivo. Because CD34 is lost upon BMP inhibition, it has been difficult to isolate these cells via cell sorting. We overcame this obstacle by generating BMP receptor 1A (*Bmpr1a*) floxed mice using a keratin 15 promoter (K15)-driven recombinase (Cre) conjugated to a truncated progesterone receptor (PR) (K15CrePR) (Fig. S1*A*) (7). Along with specific inactivation of BMP signaling in hfSCs, we simultaneously labeled hfSCs by crossing these mice with a Cre-dependent YFP (yellow fluorescent protein) reporter knocked into the ubiquitously expressed Rosa26 locus (R26YFP) (Fig. S1*A*) (24). Offspring from matings of K15CrePR/*Bmpr1a*(fl/+)/YFP(fl/+) mice yielded litters of the expected numbers, genotype, and Mendelian ratios (Fig. S1 *B* and *C*). RU486 (RU) was applied topically to back skin (BS) of adult mice to induce Cre-dependent recombination when HFs were in the second extended and synchronized postnatal telogen at postnatal day 43 (P43) (Fig. 1*A*) and were indistinguishable at the end of RU treatment at P59 (Fig. 1 *B* and *E*).

Author contributions: E.K. and K.K. designed research; E.K., Y.L., and K.K. performed research; R.W. and C.-M.C. contributed new reagents/analytic tools; E.K., Y.-B.C., R.W., C.-M.C., and K.K. analyzed data; and E.K. and K.K. wrote the paper.

The authors declare no conflict of interest.

This article is a PNAS Direct Submission.

[1]To whom correspondence should be addressed. E-mail: kkobiela@med.usc.edu.

This article contains supporting information online at www.pnas.org/lookup/suppl/doi:10.1073/pnas.1121312110/-/DCSupplemental.

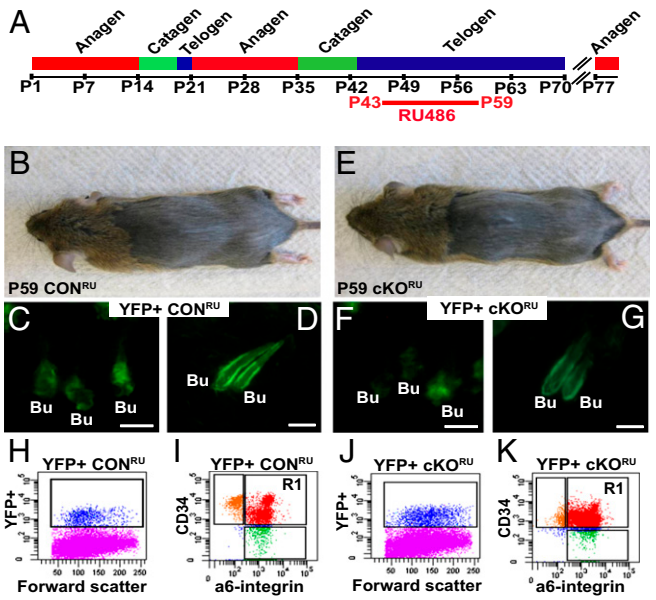

Fig. 1. Labeling and isolation hfSCs after BMP-signaling inhibition in vivo. (*A*) Chart illustrating the first and second postnatal hair cycles with RU administration. (*B* and *E*) CON^{RU} and cKO^{RU} mice showed no differences phenotypically at the end of RU treatment (P59). (*C* and *F*) Whole-mount back-skin view of the dermis from CON^{RU} and cKO^{RU} mice showing specific activation of YFP in the hfSCs after 16 d of RU treatment. (*D* and *G*) Sections through the HFs from CON^{RU} and cKO^{RU} skin showing YFP-positive bulges in telogen. (*H* and *J*) Isolation of YFP+ CON^{RU} and cKO^{RU} bulge cells from whole-mount back skin by FACS. (*I* and *K*) YFP+ fractions from CON^{RU} and cKO^{RU} were further gated into three distinct subpopulations: YFP+ CD34+ (suprabasal hfSCs); YFP+ α6+ CD34+ (basal hfSCs, R1 gates) and YFP+ α6+. Bu, bulge; RU, RU486. (Scale bars: 50 μm.)

Before RU treatment, K15CrePR^{RU}/*Bmpr1a*(fl/fl)/YFP(fl/+) or K15CrePR^{RU}/*Bmpr1a*(fl/fl)/YFP(fl/fl) (cKO) were indistinguishable from control (CON) animals. As expected, RU inducible conditional knockout (cKO^{RU}) mice at P120 showed a strong phenotype with visible hair loss [Fig. S1*E* vs. Fig. S1*D*, control after RU treatment (CON^{RU})], which confirmed high recombination efficiency in vivo (12). At P59, after 16 d of RU treatment, activated YFP expression in both cKO^{RU} (Fig. 1 *F*–*G*) and CON^{RU} (Fig. 1 *C* and *D*) bulges displayed telogen HFs with quiescent morphology verified by BrdU incorporation into YFP+ hfSCs (Fig. S1 *G* and *F*). This was also confirmed by fluorescence-activated cell sorting (FACS) analysis, checking selective BrdU incorporation into YFP-positive hfSCs at P59 (Fig. S1 *J*–*K*′). However, at P62, cKO^{RU} follicles displayed precocious anagen activation with numerous BrdU-labeled cells in the bulge and HG (Fig. S1*I*), whereas CON^{RU} HFs were still in telogen (Fig. S1*H*). Thus, before morphological changes occurred at P59, we isolated YFP+ hfSCs from cKO^{RU} or CON^{RU} by FACS (Fig. 1 *J* and *H*, respectively). Approximately 1–2% of the whole BS cell population was YFP+. These YFP+ cKO^{RU} or CON^{RU} hfSC populations were then fractionated into three distinct subpopulations by using α6-integrin and CD34 antibody staining as previously described (6): YFP+ α6+; YFP+ CD34+ (suprabasal hfSCs) and YFP+ α6+ CD34+ (basal hfSCs, marked by R1 gate) (Fig. 1 *K* and *I*, R1 gates, respectively). Although morphologically the HFs remained in telogen phase, upon BMP signaling inactivation, hfSC CD34 marker expression was decreased in cKO^{RU} cells (Fig. S1*M*), compared with CON^{RU} YFP+ CD34 high fractions (Fig. S1*L*). This was confirmed by immunofluorescent staining for CD34 (compare Fig. S1 *O* and *Q* with Fig. S1 *N* and *P*).

Reducing BMP Signaling in hfSCs Induces Hair Germ-Like Molecular Characteristics. To characterize target genes relevant for BMP signaling, total RNAs from cKO^{RU} and CON^{RU} basal hfSC populations (b-hfSCs; YFP+ α6+ CD34+; Fig. 1 *K* and *I*, R1) were used to perform microarray analysis. We confirmed that *Bmpr1a* was efficiently targeted in cKO^{RU} hfSC populations by RT-PCR detection of an exon 2 deletion in the sorted YFP+ b-hfSCs fraction (Fig. S2*A*). In our microarray dataset, we first focused on changes in the signature genes commonly up-regulated in quiescent hfSCs (5, 6, 10, 25). Inhibition of BMP signaling in the hair bulge resulted in the down-regulation of 103 gene probes (~24%) whereas only 16 of 426 probes tested (~4%) were up-regulated (Table S1). We then investigated potential similarities between cKO^{RU} hfSCs and the HG by performing immunostaining against P-cadherin (Pcad), which is highly expressed by

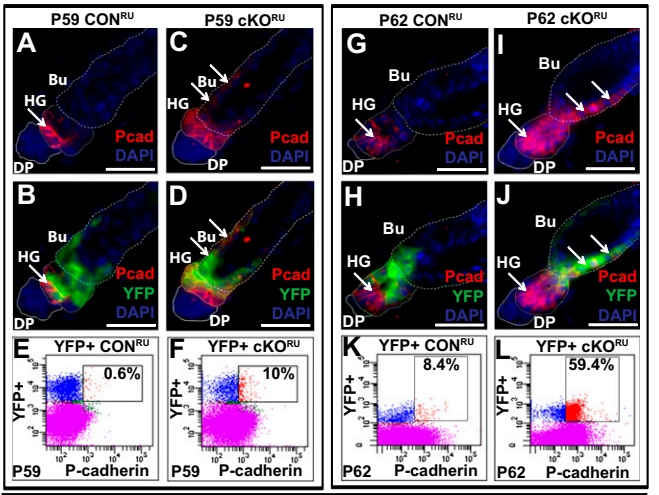

M **Hair Germ Signature**

	Down-regulated genes	Up-regulated genes
Cell Cycle	Arrest: Pmp22(-9x), Nbl1(-6x; -2x), Gas1(-3x);Sesn1(-2x)	Progression: Gsg2(30x), Mki67(14x) Cks2(11x), Ccnb1-rs1(9x), Ccnb1(9x; 2x), Ccna2(8x), Cdc2a(5x), Ccnl1(4x) Ccnb2(4x), Ccnd2(4x), Wee(4x), Ccnl2(3x), Csnk2a2(3x), Ccnd1(2x)
Signaling	FGF18(-239x; -6x), Sfrp(-73x; -2x), BMP6(-37x; 3x), Grem1(-18x; -3x), Fzd2(-15x; -4x; -2x; -2x), Ppa2a(-15x; -2x; -2x), Dkk3(-9x; -3x; -3x), Sema3e(-7x), Fzd7(-5x), Lgr5(-5x; -9x; -5x), Ltbp2(-4x; -11x), Ltbp3(-3x; -3x), Ltbp4(-3x), Fzd3(-3x; -2x; -2x), Fst(-2x)	Areg(223x; 5x), Ptgs1(90x), Wnt5a (49x), S100A8(49x; 6x), S100A9(34x; 5x), Wnt16(26x; 2x), Clca1(21x), Clca2(11x), HbEGF(20x; 7x; 4x), Lrp4(7x), Map4K5(6x), Ptgs2(5x), Map3K12(5x), Hmgn3(3x), Axin2(3x), Wnt10a(2x), Wnt4a(2x)
Transcription Factors	Id2(-52x; -9x; -2x), Lhx2(-9x), NFATc1(-8x; 2x), Sox9(-6x), Id3(-5x; -3x), Id4(-5x), Vdr(-3x), Tcf3(-3x), Nfib(-2x)	Sox6(37x), Ovo1(24x), Ap2y(16x), Sox7(6x), Sox4(5x), Cox5a(3x), Mybl2(3x), Fosb(3x; 3x), Skp2(3x), Klf5(3x), Gata(3x)
ECM / Cell Adhesion	CD34(-776x; -5x), Col6a1(-26x; -3x), Ecm1(-9x; -2x), Pnf2(-5x), cdh13(-4x), S100A6(-3x), Macf1(ACF7)(-2x)	Cdh4(6x), Col16a1(4x), Col20a1 (3x; -6x; -3x), Col4a5(2x)

Overlapping cKO^{RU}/HG down-regulated gene
Oppositely regulated cKO^{RU}/HG gene
Overlapping cKO^{RU}/HG up-regulated gene
Overlapping Wnt/HG up-regulated gene
Overlapping cKO^{RU} / Wnt HG up-regulated gene

Fig. 2. hfSCs after BMP inhibition in vivo switch from quiescence to activation and acquire molecular characteristics resembling the HG. (*A*–*B* and *C*–*D*) At P59, in CON^{RU} HFs, strong P-cadherin staining was restricted to the HG and did not overlap with YFP+ cells in the bulge (arrows). In the bulge of cKO^{RU} HFs, P-cadherin staining was expanded and increased with overlapping expression observed by YFP+ cells in both the HG and the bulge (arrows). (*I*–*J* and *G*–*H*) At P62 in the bulge of cKO^{RU}, elevated P-cadherin correlated with YFP activation (arrows), whereas, in the CON^{RU} bulge, P-cadherin staining was absent. (*E*–*F* and *K*–*L*) At P59 and P62, FACS analysis confirmed increased P-cadherin staining in YFP+ cKO^{RU} hfSCs compared with CON^{RU}, respectively. (*M*) Changes in the pool of HG signature genes in cKO^{RU} hfSCs were either up-regulated (red type) or down-regulated (green type). Only three genes characterized in cKO^{RU} hfSCs were inversely regulated, namely BMP6, NFATc1, and Col20α1 (marked in blue). (Scale bars: 50 μm.)

the HG (10). At P59, strong Pcad staining was restricted to the CON^{RU} HG with the majority of bulge cells expressing YFP alone (Fig. 2 *A* and *B*), whereas Pcad staining was expanded in the cKO^{RU} bulge and overlapped with activated YFP+ HG and bulge cells (Fig. 2 *C* and *D*). Furthermore, 3 d later at P62, stronger Pcad staining in the cKO^{RU} bulge correlated with YFP activation (Fig. 2 *I* and *J*), whereas the CON^{RU} bulge remained Pcad-negative (Fig. 2 *G* and *H*). These findings were confirmed using FACS analysis at P59 (Fig. 2 *E* and *F*) and P62 (Fig. 2 *K* and *L*). Then we tested changes in the pool of HG signature genes in cKO^{RU} hfSCs (10). Our data demonstrated that cKO^{RU} hfSCs acquire some molecular characteristics resembling the HG; 32% of the previously characterized HG signature genes were either up- or down-regulated following BMP inhibition (Fig. 2*M*; genes in red and green type, respectively; Table S2). Surprisingly, only three genes characterized in cKO^{RU} hfSCs did not follow similar changes observed in the HG signature genes. In fact, BMP6, NFATc1, and Col20α1 were inversely regulated (Fig. 2*M*; genes in blue type; Table S2). These changes in gene expression were verified by real-time PCR using independent FACS-isolated biological samples (Fig. S3).

BMP-Inactivated Stem Cells Retain Multipotentiality. We then evaluated the self-renewing capacity of FACS isolated and cultured b-hfSCs from cKO^{RU} and CON^{RU} (Fig. S2*B*). After initially similar attachment rates (Fig. S2*C*, 24 h) over a period of 7 d, cKO^{RU} hfSCs displayed a faster proliferation rate with a larger overall colony size (defined as more than four cells) over CON^{RU} hfSCs (Fig. S2*B*, days 3–7 and Fig. S2*C*, day 7 and FACS). Indeed, although colony-forming efficiency was relatively similar during the first 3 d (Fig. S2*D*), cKO^{RU} hfSC colonies were significantly larger than CON^{RU} ones with a higher average cell number per colony (Fig. S2*E*). Both cKO^{RU} and CON^{RU} hfSC lines could be passaged multiple times (>20 passages). Next, we checked if cKO^{RU} hfSCs retained multipotency characteristics and regenerative potential in vivo by performing chamber graft experiments (Fig. S2*F*) (26). Cultured YFP+ hfSCs from both cKO^{RU} and CON^{RU} were mixed with freshly isolated newborn dermal fibroblasts and engrafted into athymic mice (Fig. 3 *A* and *F* and Fig. S2*F*). Following removal of the chamber dome 2 wk after engraftment, the grafts became covered by YFP+ epidermis (Fig. 3 *B* and *G*), indicating survival of the hfSCs (Fig. 3 *C* and *H*). At 8 wk post engraftment, we observed visible hair (with shafts) on the surface of the CON^{RU} but not the cKO^{RU} grafted regions (Fig. 3 *D* and *I*, respectively). However, graft cryosections revealed that YFP+ hfSCs from cKO^{RU} and CON^{RU} retained multipotency by regenerating YFP+ epidermis and HFs in vivo, although cKO^{RU} hair shaft formation was compromised (Fig. 3 *J* and *E*).

Altered Gene Profile in BMP-Inactivated Stem Cells Reveals a Dynamic Molecular Equilibrium Within hfSCs. Both BMP and Wnt signaling are known to be crucial for hfSC homeostasis regulation (5, 7, 12, 23, 25, 27). Therefore, we looked for changes in our cKO^{RU} hfSC microarray data and found profoundly altered expression of genes involved in both pathways (Fig. 4*A*). The majority of these gene changes were consistent with patterns of gene expression obtained from another microarray dataset generated using independent biological samples from the whole fractions of YFP+ CON^{RU} and cKO^{RU} hfSCs (Fig. 4*A*). These data were confirmed by qPCR (Fig. 4*B*). After initial BMP inactivation, we observed down-regulation of Gremlin and Bambi (BMP antagonists) and up-regulation of BMP6 (BMP agonist). Additionally, Wnt signaling-associated genes such as Dkk3, Fzd2, and Fzd3 (up-regulated in hfSCs) (5–7) were down-regulated in cKO^{RU} hfSCs (Fig. 4*A*). Genes proposed to be direct targets of BMP signaling, *Id2* and *Id3* (28, 29), and known to be up-regulated in hfSCs (5–7), were consistently down-regulated in cKO^{RU} hfSCs (Fig. 4 *A* and *B*). Unexpectedly, BMP inhibition in hfSCs up-regulated the expression of three other Wnt ligands: Wnt7a, Wnt7b, and Wnt16, previously not described to play a role in hfSC regulation. This was accompanied by activation of only one Wnt receptor, Fzd 10 (Fig. 4*A*). We focused on Wnt7a and confirmed its up-regulation in cKO^{RU} hfSCs by qPCR in independent FACS-sorted YFP+ biological samples (Fig. 4*B*). Immunostaining localized the up-regulated Wnt7a to the bulge and HG of cKO^{RU} hfSCs at P59 (Fig. 4*D*, arrows) whereas CON^{RU} hfSCs remained negative (Fig. 4*C*). During precocious anagen in cKO^{RU} hfSCs at P62, we observed stronger Wnt7a staining in both the HG and the bulge over negative CON^{RU} (Fig. 4 *H* and *G*, arrows, respectively). It correlated well with stabilized nuclear β-catenin staining in cKO^{RU} hfSCs at both P59 and P62 (Fig. 4 *F* and *J*) whereas telogen CON^{RU} hfSCs remained negative (Fig. 4 *E* and *I*). We confirmed that Wnt7a was present in the bulge and HG during the physiological onset of anagen at P21 (Fig. 4*M*). This staining was negative in telogen HFs at P18 (Fig. 4*K*). Again there was a correlation with stabilized nuclear β-catenin staining in the hfSCs (Fig. 4 *N* vs. *L*).

In contrast, the normal up-regulation of Wnt7a at P21 was fully inhibited in FACS-sorted K15-GFP+/double-transgenic (dTg) hfSCs (Fig. S4*A*) (12) after in vivo BMP pathway activation produced by 3 d of doxycycline (Doxy) treatment (Fig. S4*B*, Dox; Fig. 4*O*, P21 vs. P21+Dox). This was confirmed by qPCR. Skin sections showed that anagen onset was blocked in K15-GFP+/dTg (Fig. S4 *D′* vs. *D* and *C*, P21 and P18), keeping the skin in a prolonged telogen (Fig. S4 *E′* vs. *E*, P25). Long-term Doxy treatment of these mice resulted in baldness (Fig. S4 *G′* vs. *G*). Chromatin immunoprecipitation (ChIP) assays of P21 FACS-isolated K15-GFP+/dTg hfSCs (Fig. S4*D′*) confirmed that BMP activation results in Phospho-Smads (P-Smads) directly binding to the *Wnt7a* promoter and to a known control target, Id2 (Fig. 4*T*). These interactions were not detected in P21 control hfSCs at anagen onset (Fig. 4*T*). In addition, nonspecific IgG precipitations were also negative (Fig. 4*T*). Additionally, at P25, after 7 d of BMP activation by Doxy treatment, K15-GFP+/dTg HFs exhibiting K15-GFP in the bulge region remained in telogen (Fig. S4*E′*). In contrast, control hfSCs had transitioned into

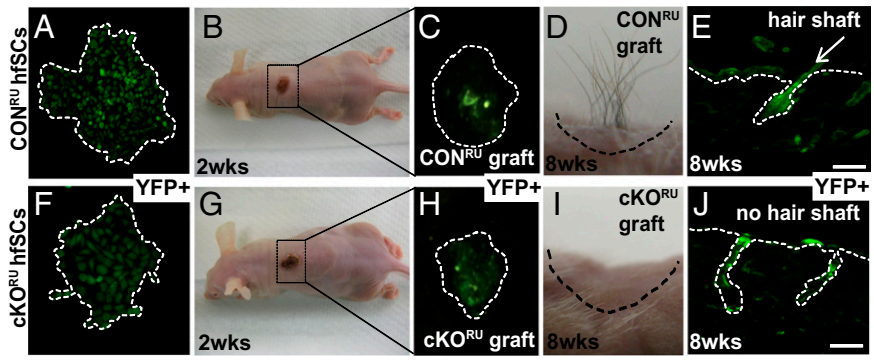

Fig. 3. hfSCs without BMP signaling maintain stem cell characteristics and their multipotency in vivo. (*A* and *F*) Cultured YFP+ hfSCs from CON^{RU} and cKO^{RU} HFs were mixed with freshly isolated dermal fibroblasts from newborn mice (1:1 ratio) and engrafted into athymic mice (*B*, *G*, *C*, and *H*). Two weeks after engraftment both grafted regions from CON^{RU} and cKO^{RU} were healed and covered by YFP+ epidermis. (*D* and *I*) Eight weeks after engraftment, the CON^{RU} but not cKO^{RU} grafted region presented visible hair shafts on the skin surface. (*E* and *J*) Skin sections of the CON^{RU} and cKO^{RU} grafts showed YFP+ epidermis and HFs, but the cKO^{RU} grafts lacked differentiated hair shafts. In vitro and in vivo experiments were repeated in triplicate ($n = 3$) using two independent FACS-isolated cell lines for both the cKO^{RU} and CON^{RU} hfSCs. (Scale bars: 50 μm.)

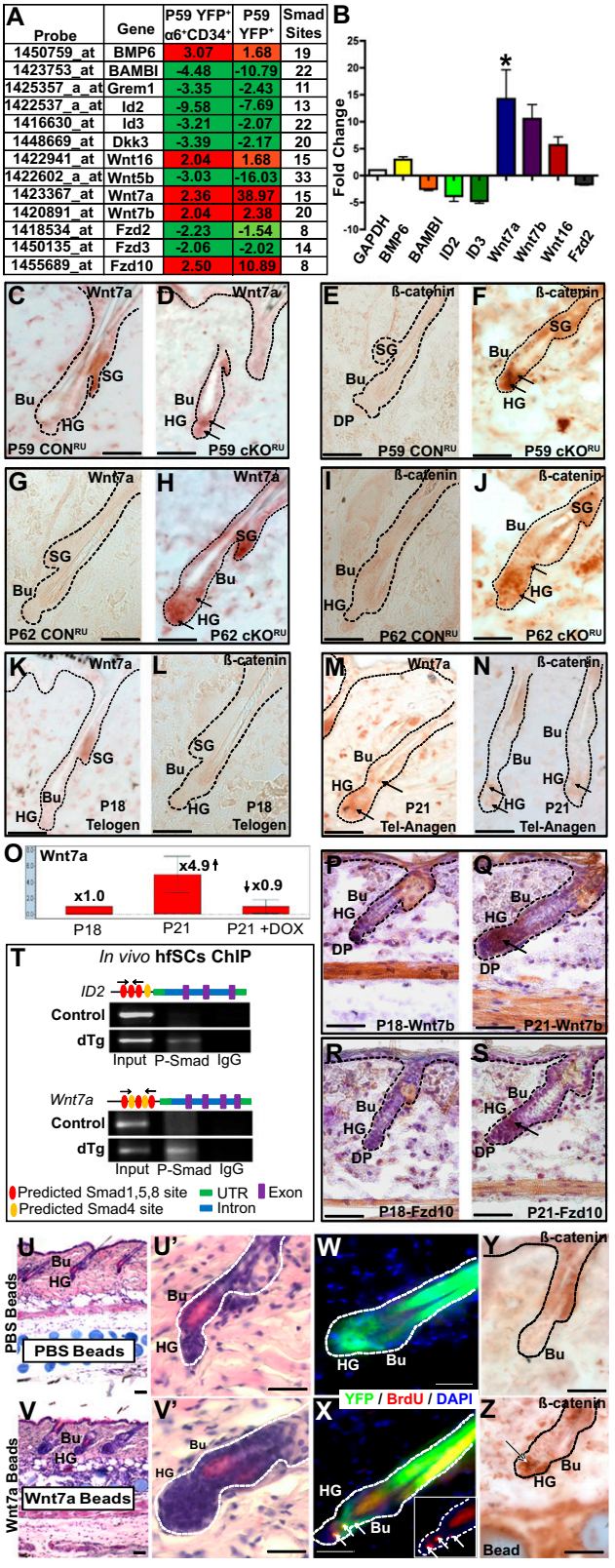

Fig. 4. Intrinsic changes in gene expression of BMP and Wnt signaling in hfSCs upon BMP inhibition. Subcutaneous injection of Wnt7a induces precocious telogen-to-anagen transition. (*A*) Microarray datasets of P59 cKO^{RU} b-hfSCs (YFP + α6+ CD34+ subpopulation) and cKO^{RU} YFP+ hfSCs from two independent biological samples showed similar expression patterns of genes involved in both the BMP and Wnt pathways. (*B*) qPCR analysis confirmed microarray data, using FACS-sorted YFP+ CON^{RU} and cKO^{RU} hfSCs at P59. (*C* and *D*) Wnt7a protein staining was up-regulated in the bulge and HG of cKO^{RU} but not present in CON^{RU} hfSCs at P59 when HFs remained in telogen (arrows). (*G* and *H*) At P62, when precocious anagen takes place in cKO^{RU} HFs, strong Wnt7a staining is found in both the bulge and the HG regions of cKO^{RU} HFs, but not in the CON^{RU}. (*F* and *J*) Nuclear β-catenin staining in cKO^{RU} hfSCs at P59 and P62. (*E* and *I*) No nuclear β-catenin staining was visible in CON^{RU} hfSCs at P59 and P62. (*M* and *K*) Wnt7a staining was present at the onset of the physiological anagen at P21 in the bulge and HG, but not at P18 telogen HFs. (*N* and *L*) At P21, physiological up-regulation of Wnt7a staining correlated with nuclear β-catenin staining in bulge hfSCs, but no nuclear β-catenin stabilization was observed in telogen HFs at P18. (*O*) qPCR analysis showed a physiological ~5×-fold increase in Wnt7a gene expression between P18 and P21 in FACS-sorted GFP+ hfSCs without Doxy treatment. After activation of BMP signaling by Doxy treatment in hfSCs at P18, Wnt7a up-regulation was inhibited at P21. (*Q* and *S*) Wnt7b and Fzd10 up-regulation in the P21 bulge and HG at physiological telogen–anagen transition, respectively. (*P* and *R*) At telogen P18, controls remain negative in HG and bulge. (*T*) In vivo ChIP PCR reveals selective precipitation of DNA fragments that possess canonical Smad-binding motifs. Schematic representation of primers designed to flank conserved Smad-binding elements within the promoter regions of mouse ID2 and Wnt7a. (*U* and *V*) H&E staining after s.c. injection of Wnt7a- or PBS-coated agarose beads during the second telogen showed increased HG size of HFs in proximity to Wnt7a-coated beads, but HFs adjacent to PBS-coated agarose beads remained in telogen. (*U′* and *V′*) Higher magnification of the H&E staining from *U* and *V*. (*X* and *W*) At P62, Wnt7a-treated HFs displayed BrdU-labeled HG and lower bulge cells (arrows), whereas no BrdU incorporation was visible in PBS-treated control HFs. (*Z* and *Y*) The lower bulge hfSCs and most of the HG adjacent to the Wnt7a-soaked beads showed nuclear β-catenin staining, whereas PBS control HFs remained negative. (Scale bars: 50 μm.)

anagen (Fig. S4*E*, *Inset*). At this time point, flow cytometry revealed more P-Smad–positive cells in K15-GFP+/dTg (Fig. S4*F′*) than in anagen K15-GFP+/control hfSCs (Fig. S4*F*). We further confirmed that other Wnt pathway components identified in our microarray, such as Wnt7b and Fzd10 (Fig. 4*A*), were also expressed at the protein level in the bulge and HG during physiological anagen activation at P21 (Fig. 4 *P*–*S*).

Augmentation of Wnt Signaling by Ectopic Wnt7a Induces Precocious Activation of hfSCs. Recently, s.c.-injected Wnt7a soaked beads were shown to promote nuclear β-catenin stabilization in the HG of epithelial stem cells (EpSCs) and melanocyte stem cells (McSCs) (30). However, that research did not show whether Wnt7a promoted hfSC and HG activation as well as self-renewal. Thus, to test the functional significance of Wnt7a expression in hfSC homeostasis in vivo, we s.c.-injected CON mice with PBS (control) or recombinant Wnt7a-coated agarose beads during the second prolonged quiescent telogen (Fig. S5*A*). After 5 d of daily bead injections evaluated at P59 and P62, H&E staining revealed an increased HG size in HFs in close proximity to the Wnt7a-coated beads (Fig. 4 *V* and *V′* and Fig. S5*C*), showing morphological signs of precocious synchronized hfSC activation (>90% of HFs). In contrast, controls remained in telogen (Fig. 4 *U* and *U′* and Fig. S5*B*). To test this possibility further, we administered 3-h pulses of BrdU before skin samples were processed. At P59, Wnt7a-treated HFs displayed numerous BrdU-labeled HG and lower bulge cells (Fig. 4*X*, *Inset*, arrows), whereas PBS-treated control HFs were in telogen without any visible bulge/HG cells incorporating BrdU (Fig. 4*W*). The proliferation status of HFs after ectopic Wnt7a exposure was also confirmed by proliferating cell nuclear antigen (PCNA) staining at P62 (Fig. S5*E*). PCNA staining was negative in control HFs (Fig. S5*D*). In addition, we confirmed triple-positive staining for Ki67 staining, CD34, and YFP in the lower bulge region (Fig. S5*G*), whereas control telogen HFs remained Ki67-negative (Fig. S5*F*). Consequently, with concomitant synchronized hfSCs activation, nuclear β-catenin stabilization was observed in lower bulge hfSCs, predominantly in the HG adjacent to Wnt7a-soaked beads. This demonstrates that canonical Wnt pathway induction occurs precociously in the HG and lower bulge hfSCs in response

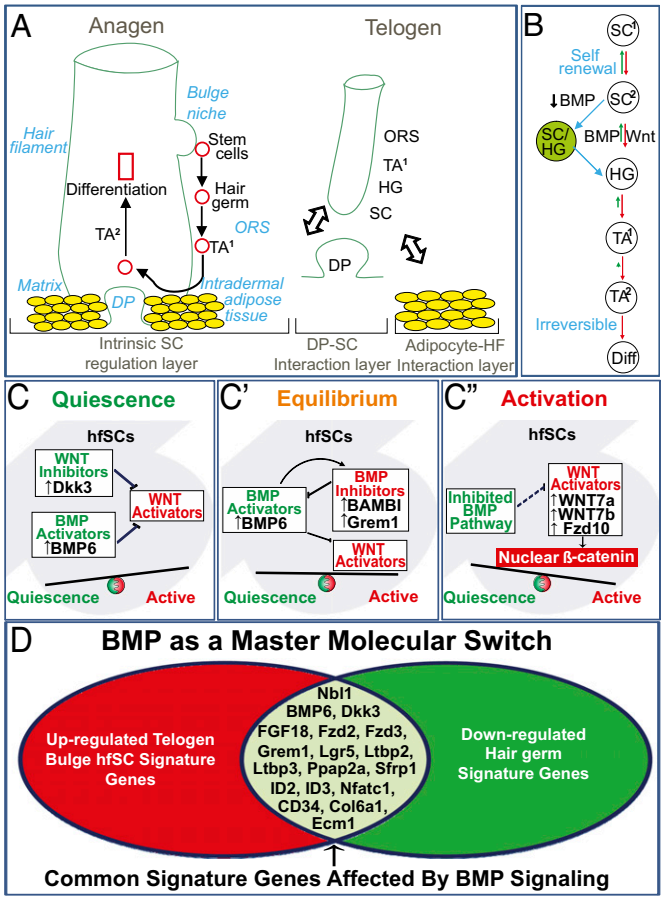

Fig. 5. Model of intrinsic mechanism of ligand–receptor-dependent cross talk between BMP and Wnt signaling in hfSC homeostasis regulation. (*A*) An intrinsic SC regulation layer acts as a third hierarchical layer regulating hfSC homeostasis along with the DP–SC interaction layer and HF–adipocyte interaction layer. (*B*) Schematic of transient activated hfSCs after BMP inhibition reflects a new SC/HG status that shares properties between SC and HG states and may be very temporary in vivo. (*C*–*C*″) Proposed hypothesis of intrinsic constant competitive cycling between activator (Wnt) and inhibitor (BMP) activities in bulge hfSCs. (*D*) Common signature genes between bulge and HG affected by BMP signaling, which works as a master switch. Diff, differentiated cells; HG, hair germ; SC, stem cell; TA, transit amplifying.

to exogenous Wnt7a ligand (Fig. 4*Z*) whereas the PBS control remains negative (Fig. 4*Y*).

Discussion

Here we demonstrate the salient features of the hfSC gene network. We show how the delicate balance between BMP and Wnt activity within each bulge stem cell can maintain stem cell status in a state ready to be activated toward hair germ fate upon reduction of BMP signaling or enhanced Wnt signaling. On the other hand, excessive BMP signaling, whether derived from an intra- or extrafollicular source, can lock hfSCs in quiescent states, as observed in refractory telogen. Such a competitive equilibrium is at the core of this unique stem cell gene network module, making it able to sense multilayered environmental regulation (Fig. 5*A*) to reversibly tilt toward either activation or quiescent states (Fig. 5 *C*–*C*″).

Characterization of BMP-Inactivated hfSC Reveals a Molecular Module Capable of Switching Back and Forth Between Activated and Quiescent States, Allowing Cyclic Regeneration. Our results demonstrate that more than 50% of all down-regulated signature genes in the HG (18 of 35 genes) were affected by BMP inhibition (Figs. 2*M* and 5*D*; Fig. S6; Table S2). Strikingly, all of these BMP-dependent down-regulated HG genes are signature genes of the quiescent bulge (Fig. 5*D*; Fig. S6; Table S2). This shows that inhibition of BMP signaling in the bulge works as a "switch" to activate quiescent hfSCs in a very defined and synchronized manner, instructing these cells to partially adopt an intermediate active state resembling the HG (Fig. 5*D*). Interestingly, in cKO^{RU} hfSCs, three genes—BMP6, NFATc1, and Col20α1—did not adopt the early HG signature expression pattern and were inversely regulated (Fig. 2*M*; genes in blue). This suggests an auto-regulatory feedback loop after BMP inhibition, which could work as a very early mechanism to reversibly inhibit hfSCs and return them to a quiescent state, preventing consequences of hfSC overactivation. That is consistent with previously published data reporting that BMP6 and NFATc1 were involved in SC quiescence along with FGF18, which has the opposing trend in our array (10). Although cKO^{RU} cells acquired HG-like gene profiles, these cells maintain multipotency in vivo (Fig. 3 and Fig. S2). Thus, this experimental condition reflects a status between the SC and HG states (Fig. 5*B*), which may be very transient in vivo. One attractive scenario in light of two recently published reports (31, 32) is that these cells may be activated to exit the old bulge and transiently adopt characteristics of upper outer root sheath (ORS) cells in the direct vicinity of the old bulge. It will be interesting to test these possibilities in the future.

Putting our and other's work together, we can appreciate that the hfSC gene network is capable of tilting toward either the activated or the quiescent state and that such conversion is reversible when the activator/inhibitor ratio is balanced, but gradually can become committed toward either extreme (Fig. 5 *C*–*C*″).

Cellular-Autonomous Loop Regulates BMP Signaling Within hfSCs. Our system gives us a unique opportunity to look at hfSC properties directly at early time points of the telogen–anagen transition. Surprisingly, hfSCs with suppressed BMP signaling revealed profound altered expression in the BMP pathway itself. These data led us to propose a model (Fig. 5 *C*–*C*″) in which BMP inhibition in hfSCs leads to a cell-autonomous secretion of BMP6 and suppression of the BMP antagonists Gremlin and Bambi (Fig. 4 *A* and *B*). Our data indicate that the initial consequences of BMP inactivation will be the temporal activation of hfSCs in telogen HFs (Fig. 5*C*″). Then, these activated hfSCs will gradually start to re-express the BMP agonist, BMP6 (Fig. 5*C*), which correlates with the simultaneous inhibition of the BMP antagonists Gremlin and Bambi. The feedback loop will then reverse after BMP reaches full activation in hfSCs, resulting in progressive activation of their own antagonists, Gremlin and Bambi, completing the cycle (Fig. 5*C*′). In this way, cyclic regulation of agonists (e.g., BMP6) or antagonists (e.g., Bambi, Grem1) is directly regulated by BMP canonical signaling in hfSCs.

Cross Talk Between BMP and Wnt Signaling Gives hfSCs Unique Flexibility to Integrate Multilayered Signaling Inputs. Although the role of β-catenin in hfSCs was discovered more than a decade ago, whether canonical Wnt-signaling activation is ligand(s)-dependent or -independent still remains elusive. Here, our data propose an intrinsic mechanism of hfSC regulation whereby BMP inhibition regulates ligand–receptor-dependent canonical Wnt activation (Fig. 5 *C*–*C*″). The data suggest that, after the initial BMP inactivation, there is intrinsic activation of Wnt7a, Wnt7b, and Wnt16 ligands in hfSCs, whereas the Wnt antagonist Dkk3 is suppressed (Figs. 4 *A* and *B* and 5 *C*–*C*″). At the same time, the expression of Wnt receptor Fzd10 is increased. Thus, the decrease of BMP signaling unleashes Wnt pathway activation via ligand and receptor up-regulation and antagonist down-regulation.

Is the Wnt activation effect generic or specific? The role of Wnt7a as an activator for hair regeneration is further evaluated. Overexpression of Wnt7a in K14-Wnt7a transgenic mice shows enhanced HF neogenesis after wounding (33). K14-Wnt7a mice exhibit shortened telogen and continuous propagation of regenerative waves (14). Wnt7a-soaked beads cause precocious nuclear β-catenin stabilization in EpSCs and McSCs (30). Wnt7a can also mediate epidermal–mesenchymal interactions as it is

important in maintaining the HFs inducing activity of cultured DP cells (34). Other Wnts such as Wnt10b were visualized in the lower, permanent portion of the follicular epithelium (*ISH*) (27, 30). The exogeneous delivery of Wnt10b can lead to anagen activation (35). The stem cell module here may be able to sense different Wnts as activators, and we will focus more on the increase of β-catenin activity in hfSC, rather than on specific Wnts.

Is increased Wnt signaling a direct effect of BMP inactivation or a consequence of hair germ activation? We consistently observed Wnt ligand and receptor expression changes immediately following BMP inactivation in quiescent hfSCs (Fig. 4 *A* and *B* and Fig. S1 *F–G* and *J–K′*), when most of the canonical Wnt signaling target genes were not yet affected (Fig. 2*M*, overlapping Wnt/HG up-regulated genes, in brown) (10, 25). At this early point, only one gene, cyclin B1 (ccnb1), overlapped between the Wnt and BMP pathways following BMP inhibition in hfSCs (Fig. 2*M*, overlapping $cKO^{RU}$and Wnt/HG up-regulated genes, underlined in brown). This delayed activation of most canonical Wnt-dependent cell cycle target genes after BMP inactivation is consistent with our model emphasizing that BMP inhibition precedes ligand–receptor-dependent canonical Wnt up-regulation and hfSC activation.

Finally, we wonder if BMP regulation of Wnt is at the transcriptional level. We were able to repress Wnt7a in vivo using our BMP gain-of-function, inducible K15-GFP+/dTg system (Fig. 4*O*, P21+Dox) and confirmed direct binding of P-Smads to the *Wnt7a* promoter in vivo in FACS-isolated hfSCs by ChIP assay (Fig. 4*T*) when HFs remained in a BMP-induced telogen at P21 (Fig. S4*D′*).

In summary, we are able to demonstrate the key role of BMP signaling and its cross talk in the gene network governing the homeostasis of hfSCs. Inactivation of BMP signaling in K15-positive bulge stem cells reveals intracellular cross talk between the BMP/Wnt pathways. Such dynamic balance confers hfSCs with a robust ability to regenerate cyclically and to sense generic activators and inhibitors when deciding whether to activate or not.

Materials and Methods

Mice and RU486 Treatment Time Line. All mice were housed and bred within the animal facility at the University of Southern California in accordance with the Institutional Animal Care and Use Committee (Protocol 11543). A series of matings were set up using $Bmpr1a^{fl/fl}$ mice (36), K15-CrePR1 mice (7), and Rosa26-STOP-eYFP (24) mice to generate offspring $Bmpr1a^{+/+}$ (control, CON), $Bmpr1a^{fl/+}$(CON), or $Bmpr1a^{fl/fl}$ (knockout, cKO) mice, which were genotypically positive for K15CrePR and Rosa-STOP-eYFP. Targeting was achieved by daily application of 2.5 mg/mouse RU486 [(wt/vol) in 100% ethanol; VWR] for 16 d to shaved back skins at P43 (corresponding to the start of the second postnatal telogen) and ending at P59.

Mice and Doxy Treatment Time Line. Previously generated doxycycline (Doxy)-inducible double-transgenic (dTg) mice that express a constitutively active form of *Bmpr1a* gene (12) were crossed in the background of K15-GFP reporter mice (37). GFP+ hair follicle stem cells (hfSCs) for quantitative PCR (qPCR) analysis were sorted by FACS from either untreated or Doxytreated (3 d) postnatal day 21 (P21) mice.

ACKNOWLEDGMENTS. We thank Dr. Richard R. Behringer (MD Anderson Cancer Center) for floxed-*Bmpr1a* mice and Dr. Peggy Farnham (University of Southern California) for help with ChIP assay optimization. We thank the Genomics Core Facility, Children's Hospital Los Angeles, and the University of Southern California Flow Cytometry Core and Animal Facility for mouse husbandry. E.K. is a fellow of the California Institute for Regenerative Medicine (CIRM)–Research Training Program II in Stem Cell Biology. This work was supported initially by the Donald E. and Delia B. Baxter Foundation Award (to K.K.) and National Institute of Arthritis and Musculoskeletal and Skin Diseases of the National Institutes of Health Grants R01-AR061552 (to K.K.), AR42177 (to C.-M.C.), and AR060306 (to C.-M.C.).

1. Chuong CM, Randall VA, Widelitz RB, Wu P, Jiang TX (2012) Physiological regeneration of skin appendages and implications for regenerative medicine. *Physiology (Bethesda)* 27(2):61–72.
2. Ito M, et al. (2005) Stem cells in the hair follicle bulge contribute to wound repair but not to homeostasis of the epidermis. *Nat Med* 11(12):1351–1354.
3. Chen CC, Chuong CM (2012) Multi-layered environmental regulation on the homeostasis of stem cells: The saga of hair growth and alopecia. *J Dermatol Sci* 66(1):3–11.
4. Cotsarelis G, Sun TT, Lavker RM (1990) Label-retaining cells reside in the bulge area of pilosebaceous unit: Implications for follicular stem cells, hair cycle, and skin carcinogenesis. *Cell* 61(7):1329–1337.
5. Tumbar T, et al. (2004) Defining the epithelial stem cell niche in skin. *Science* 303 (5656):359–363.
6. Blanpain C, Lowry WE, Geoghegan A, Polak L, Fuchs E (2004) Self-renewal, multipotency, and the existence of two cell populations within an epithelial stem cell niche. *Cell* 118(5):635–648.
7. Morris RJ, et al. (2004) Capturing and profiling adult hair follicle stem cells. *Nat Biotechnol* 22(4):411–417.
8. Claudinot S, Nicolas M, Oshima H, Rochat A, Barrandon Y (2005) Long-term renewal of hair follicles from clonogenic multipotent stem cells. *Proc Natl Acad Sci USA* 102(41):14677–14682.
9. Müller-Röver S, Peters EJ, Botchkarev VA, Panteleyev A, Paus R (1998) Distinct patterns of NCAM expression are associated with defined stages of murine hair follicle morphogenesis and regression. *J Histochem Cytochem* 46(12):1401–1410.
10. Greco V, et al. (2009) A two-step mechanism for stem cell activation during hair regeneration. *Cell Stem Cell* 4(2):155–169.
11. Blanpain C, Fuchs E (2009) Epidermal homeostasis: A balancing act of stem cells in the skin. *Nat Rev Mol Cell Biol* 10(3):207–217.
12. Kobielak K, Stokes N, de la Cruz J, Polak L, Fuchs E (2007) Loss of a quiescent niche but not follicle stem cells in the absence of bone morphogenetic protein signaling. *Proc Natl Acad Sci USA* 104(24):10063–10068.
13. Plikus MV, et al. (2008) Cyclic dermal BMP signalling regulates stem cell activation during hair regeneration. *Nature* 451(7176):340–344.
14. Plikus MV, et al. (2011) Self-organizing and stochastic behaviors during the regeneration of hair stem cells. *Science* 332(6029):586–589.
15. Festa E, et al. (2011) Adipocyte lineage cells contribute to the skin stem cell niche to drive hair cycling. *Cell* 146(5):761–771.
16. Janich P, et al. (2011) The circadian molecular clock creates epidermal stem cell heterogeneity. *Nature* 480(7376):209–214.
17. Lin KK, et al. (2009) Circadian clock genes contribute to the regulation of hair follicle cycling. *PLoS Genet* 5(7):e1000573.
18. Zhang J, et al. (2006) Bone morphogenetic protein signaling inhibits hair follicle anagen induction by restricting epithelial stem/progenitor cell activation and expansion. *Stem Cells* 24(12):2826–2839.
19. Plikus M, et al. (2004) Morpho-regulation of ectodermal organs: Integument pathology and phenotypic variations in K14-Noggin engineered mice through modulation of bone morphogenic protein pathway. *Am J Pathol* 164(3):1099–1114.
20. Botchkarev VA, et al. (2001) Noggin is required for induction of the hair follicle growth phase in postnatal skin. *FASEB J* 15(12):2205–2214.
21. Andl T, et al. (2004) Epithelial Bmpr1a regulates differentiation and proliferation in postnatal hair follicles and is essential for tooth development. *Development* 131(10):2257–2268.
22. Kobielak K, Pasolli HA, Alonso L, Polak L, Fuchs E (2003) Defining BMP functions in the hair follicle by conditional ablation of BMP receptor IA. *J Cell Biol* 163(3):609–623.
23. Gat U, DasGupta R, Degenstein L, Fuchs E (1998) De novo hair follicle morphogenesis and hair tumors in mice expressing a truncated beta-catenin in skin. *Cell* 95(5):605–614.
24. Srinivas S, et al. (2001) Cre reporter strains produced by targeted insertion of EYFP and ECFP into the ROSA26 locus. *BMC Dev Biol* 1:4.
25. Lowry WE, et al. (2005) Defining the impact of beta-catenin/Tcf transactivation on epithelial stem cells. *Genes Dev* 19(13):1596–1611.
26. Weinberg WC, et al. (1993) Reconstitution of hair follicle development in vivo: Determination of follicle formation, hair growth, and hair quality by dermal cells. *J Invest Dermatol* 100(3):229–236.
27. Reddy S, et al. (2001) Characterization of Wnt gene expression in developing and postnatal hair follicles and identification of Wnt5a as a target of Sonic hedgehog in hair follicle morphogenesis. *Mech Dev* 107(1–2):69–82.
28. Nakahiro T, Kurooka H, Mori K, Sano K, Yokota Y (2010) Identification of BMP-responsive elements in the mouse Id2 gene. *Biochem Biophys Res Commun* 399(3):416–421.
29. Ho CC, Zhou X, Mishina Y, Bernard DJ (2011) Mechanisms of bone morphogenetic protein 2 (BMP2) stimulated inhibitor of DNA binding 3 (Id3) transcription. *Mol Cell Endocrinol* 332(1-2):242–252.
30. Rabbani P, et al. (2011) Coordinated activation of Wnt in epithelial and melanocyte stem cells initiates pigmented hair regeneration. *Cell* 145(6):941–955.
31. Jaks V, et al. (2008) Lgr5 marks cycling, yet long-lived, hair follicle stem cells. *Nat Genet* 40(11):1291–1299.
32. Hsu YC, Pasolli HA, Fuchs E (2011) Dynamics between stem cells, niche, and progeny in the hair follicle. *Cell* 144(1):92–105.
33. Ito M, et al. (2007) Wnt-dependent de novo hair follicle regeneration in adult mouse skin after wounding. *Nature* 447(7142):316–320.
34. Kishimoto J, Burgeson RE, Morgan BA (2000) Wnt signaling maintains the hair-inducing activity of the dermal papilla. *Genes Dev* 14(10):1181–1185.
35. Li YH, et al. (2012) Adenovirus-mediated Wnt10b overexpression induces hair follicle regeneration. *J Invest Dermatol*, 10.1038/jid.2012.235.
36. Mishina Y, Hanks MC, Miura S, Tallquist MD, Behringer RR (2002) Generation of Bmpr/Alk3 conditional knockout mice. *Genesis* 32(2):69–72.
37. Liu Y, Lyle S, Yang Z, Cotsarelis G (2003) Keratin 15 promoter targets putative epithelial stem cells in the hair follicle bulge. *J Invest Dermatol* 121(5):963–968.